


## Fermi spin polaron and dissipative Fermi-polaron Rabi dynamics

Hui Hu <sup>1</sup> and Xia-Ji Liu<sup>1,2</sup>

<sup>1</sup>Centre for Quantum Technology Theory, Swinburne University of Technology, Melbourne, Victoria 3122, Australia

<sup>2</sup>Kavli Institute for Theoretical Physics, UC Santa Barbara, Santa Barbara, California 93106-4030, USA



(Received 5 June 2022; accepted 5 December 2023; published 19 December 2023)

We consider a spin impurity with multiple energy levels moving in a noninteracting Fermi sea and theoretically solve this Fermi-spin-polaron problem at nonzero temperature by using a non-self-consistent many-body  $T$ -matrix theory. We focus on the simplest case with spin  $\frac{1}{2}$ , where the two energy states of the impurity are coupled by a Rabi flip term. At small Rabi coupling, the impurity exhibits damped Rabi oscillations, where the decoherence is caused by the interaction with the Fermi sea, as recently reported in Fermi-polaron experiments with ultracold atoms. We investigate the dependence of Rabi oscillations on the Rabi coupling strength and examine the additional nonlinear damping due to large Rabi coupling. At finite temperature and nonzero impurity concentration, the impurity can acquire a pronounced momentum distribution. We show that the momentum or thermal average can sizably reduce the visibility of Rabi oscillations. We compare our theoretical predictions to recent experimental data and find good agreement without any adjustable parameters.

DOI: [10.1103/PhysRevA.108.063312](https://doi.org/10.1103/PhysRevA.108.063312)

### I. INTRODUCTION

Quantum impurity interacting with a many-body environment is a long-lasting research topic in the modern physics [1]. The earliest study can be traced back to the seminal work by Landau [2], which led to the fundamental concept of quasiparticles. Over the past 15 years, this research topic has received renewed interest, due to rapid advances in ultracold atomic physics [3–5]. In particular, the dynamics of a quantum impurity immersed in a noninteracting Fermi sea, namely, Fermi polaron, has been systematically explored both experimentally and theoretically [6–10]. A convenient experimental setup is the use of a highly imbalanced two-component Fermi-Fermi mixture, where minority atoms in a hyperfine state can be well treated as isolated, uncorrelated impurities. For such a system, quasiparticle properties of Fermi polarons, including the ground-state attractive polaron and the excited branch of the repulsive polaron, have been well characterized experimentally by radio-frequency (rf) spectroscopy [11–16], Ramsey interferometry [17], Rabi oscillation [13,15,18], and most recently Raman spectroscopy [19]. Theoretically, an exactly solvable polaron model with a heavy impurity and a BCS superfluid environment has also been constructed [20–22], clarifying several salient features of Fermi polarons in a rigorous way.

In principle, quantum impurity can have internal degrees of freedom and can occupy multiple energy levels. For example, molecule impurity can be trapped inside a nanodroplet of superfluid helium, forming the so-called angulon quasiparticle [23]. The rotational degree of freedom of the molecule can be affected by the many-body environment of a helium droplet, as evidenced by a larger effective moment of inertia. This effect is similar to the renormalization of the effective mass for impurity observed in Fermi polarons [6]. In highly imbalanced Fermi-Fermi mixtures, it is also feasible to coherently transfer minority atoms to another hyperfine state, by using an always-on rf field [24]. Thus, impurity atoms can occupy

two different hyperfine states and acquire a pseudospin degree of freedom. Indeed, in recent Rabi dynamics experiments for Fermi polarons [13,15,18], Rabi oscillation between the two hyperfine states is driven by the rf field with reasonably small coupling strength in the linear response regime, where polaron properties are assumed to be unchanged by Rabi coupling.

In this work, we investigate in detail the Fermi spin polaron with a mobile spinor impurity, with the purpose of better understanding the Rabi dynamics of Fermi polarons. We are specifically interested in the dependence of quasiparticle properties of Fermi spin polarons on the Rabi coupling strength, which is less considered in earlier theoretical analyses on dissipative Rabi dynamics [24–26] (for an exception, see Ref. [27], where a state-of-the-art simulation of Rabi oscillations is presented). This dependence is crucial to examine the small Rabi coupling assumption adopted in recent experimental measurements [13,15,18].

Our theoretical investigation is based on a non-self-consistent many-body  $T$ -matrix theory of Fermi polarons [28–36], extended to the case of a spinor impurity. In the spinless case of a structureless impurity, such a many-body  $T$ -matrix approach is fully equivalent to Chevy's variational ansatz [37–40], including its finite-temperature extension [41]. This approach is particularly useful for a mobile impurity, whose recoil energy suppresses multiple particle-hole excitations near the Fermi surface of the many-body environment. Our results are therefore complementary to the two earlier studies [24,26], which considered the heavy impurity limit using either a spin model with an Ohmic bath [24] or the functional determinant approach [26].

Our many-body  $T$ -matrix theory is also convenient to investigate the finite-momentum effect of polarons, which arises due to the nonzero temperature and the finite impurity concentration. This effect is not emphasized in a recent Rabi dynamics study based on the finite-temperature variation approach [27], but is found to be important for understanding the measured rf spectroscopy [35]. We find that the visibility of

Rabi oscillations can be sizably reduced by the momentum average due to the thermal momentum distribution of polarons.

The rest of the paper is organized as follows. In the next section (Sec. II) we present the non-self-consistent many-body  $T$ -matrix theory for Fermi spin polarons at finite temperature. In Sec. III we discuss in detail the quasiparticle properties of spin polarons, such as self-energy, spectral function, and polaron energies, as a function of the Rabi coupling strength. We emphasize the nonlinear effect arising from large Rabi coupling. In Sec. IV we first compare our theoretical predictions with the experimental data on Rabi oscillation and show that there is good agreement, without any free fitting parameters. We then examine the effect of the momentum average and the nonlinear dependence of Rabi oscillations on large Rabi coupling strength. Finally, we give a brief summary in Sec. V.

## II. NON-SELF-CONSISTENT MANY-BODY $T$ -MATRIX THEORY

### A. Model Hamiltonian

According to the recent experiments on dissipative Rabi dynamics [13,15,18], we consider a spin- $\frac{1}{2}$  impurity of mass  $m_I$  that has two hyperfine energy levels (i.e.,  $\sigma = \uparrow, \downarrow$ ), described by the single-particle model Hamiltonian [24,26]

$$\mathcal{H}_I = \sum_{\mathbf{p}\sigma} \epsilon_{\mathbf{p}\sigma}^{(I)} d_{\mathbf{p}\sigma}^\dagger d_{\mathbf{p}\sigma} + \frac{\Omega}{2} \sum_{\mathbf{p}} (d_{\mathbf{p}\uparrow}^\dagger d_{\mathbf{p}\downarrow} + d_{\mathbf{p}\downarrow}^\dagger d_{\mathbf{p}\uparrow}), \quad (1)$$

where  $d_{\mathbf{p}\sigma}^\dagger$  and  $d_{\mathbf{p}\sigma}$  are the creation and annihilation field operators for the impurity with momentum  $\mathbf{p}$  in the spin-up ( $\sigma = \uparrow$ ) and spin-down ( $\sigma = \downarrow$ ) states that have the dispersion relations  $\epsilon_{\mathbf{p}\uparrow}^{(I)} = \epsilon_{\mathbf{p}}^{(I)} \equiv \hbar^2 \mathbf{p}^2 / 2m_I$  and  $\epsilon_{\mathbf{p}\downarrow}^{(I)} \equiv \epsilon_{\mathbf{p}}^{(I)} + \Delta$ , respectively,  $\Delta$  is the detuning, and  $\Omega$  is the Rabi coupling strength. For a spin- $\frac{1}{2}$  impurity, its noninteracting thermal Green's function is a  $2 \times 2$  matrix  $\mathbf{G}_0(\mathcal{P})$ ,

$$\begin{bmatrix} G_{11}^{(0)} & G_{12}^{(0)} \\ G_{21}^{(0)} & G_{22}^{(0)} \end{bmatrix} = \begin{bmatrix} i\omega_p - \epsilon_{\mathbf{p}}^{(I)} & -\Omega/2 \\ -\Omega/2 & i\omega_p - \epsilon_{\mathbf{p}}^{(I)} - \Delta \end{bmatrix}^{-1}, \quad (2)$$

where we have used the shorthand notation  $\mathcal{P} \equiv (\mathbf{p}, i\omega_p)$  with fermionic Matsubara frequency  $\omega_p = (2p+1)\pi k_B T$  at temperature  $T$  and integer  $p = 0, \pm 1, \pm 2, \dots$ . By diagonalizing the matrix, we find two energy levels  $E_{\mathbf{p}}^{(\pm)} = (\epsilon_{\mathbf{p}}^{(I)} + \Delta/2) \pm \sqrt{\Delta^2 + \Omega^2}/2$ . The associated amplitudes (i.e., wave functions) are given by

$$u^2 = \frac{1}{2} \left( 1 + \frac{\Delta}{\sqrt{\Delta^2 + \Omega^2}} \right), \quad (3)$$

$$v^2 = \frac{1}{2} \left( 1 - \frac{\Delta}{\sqrt{\Delta^2 + \Omega^2}} \right), \quad (4)$$

$$uv = \frac{1}{2} \frac{\Omega}{\sqrt{\Delta^2 + \Omega^2}}. \quad (5)$$

The noninteracting impurity Green's function can then be conveniently written as

$$\begin{bmatrix} G_{11}^{(0)} & G_{12}^{(0)} \\ G_{21}^{(0)} & G_{22}^{(0)} \end{bmatrix} = \frac{\begin{bmatrix} v^2 & uv \\ uv & u^2 \end{bmatrix}}{i\omega_p - E_{\mathbf{p}}^{(+)}} + \frac{\begin{bmatrix} u^2 & -uv \\ -uv & v^2 \end{bmatrix}}{i\omega_p - E_{\mathbf{p}}^{(-)}}. \quad (6)$$

The impurity is moving in and interacting with an ideal Fermi sea of fermionic atoms of mass  $m$  described by  $\sum_{\mathbf{k}} \epsilon_{\mathbf{k}} c_{\mathbf{k}}^\dagger c_{\mathbf{k}}$ , where  $c_{\mathbf{k}}^\dagger$  and  $c_{\mathbf{k}}$  are the creation and annihilation field operators for fermionic atoms with momentum  $\mathbf{k}$  and single-particle dispersion relation  $\epsilon_{\mathbf{k}} = \hbar^2 \mathbf{k}^2 / 2m$ . The total model Hamiltonian then takes the form

$$\mathcal{H} = \mathcal{H}_I + \sum_{\sigma} \frac{g_{\sigma}}{V} \sum_{\mathbf{k}\mathbf{p}\mathbf{q}} c_{\mathbf{k}}^\dagger d_{\mathbf{q}-\mathbf{k}\sigma}^\dagger d_{\mathbf{q}-\mathbf{p}\sigma} c_{\mathbf{p}} + \sum_{\mathbf{k}} \epsilon_{\mathbf{k}} c_{\mathbf{k}}^\dagger c_{\mathbf{k}}, \quad (7)$$

where  $V$  is the system volume and the middle term describes the  $s$ -wave contact interactions between the impurity and the Fermi bath with bare interaction strengths  $g_{\sigma}$ , which are to be regularized via the relation

$$\frac{1}{g_{\sigma}} = \frac{m_r}{2\pi \hbar^2 a_{\sigma}} - \frac{1}{V} \sum_{\mathbf{k}} \frac{2m_r}{\hbar^2 \mathbf{k}^2}. \quad (8)$$

Here  $a_{\sigma}$  ( $\sigma = \uparrow, \downarrow$  or interchangeably  $\sigma = 1, 2$ ) is the  $s$ -wave impurity-bath scattering length and  $m_r \equiv mm_I / (m + m_I)$  is the reduced mass. Throughout the work, we always take  $m_I = m$ , so  $m_r = m/2$ . The density  $n$  or the total number  $N = nV$  of fermionic atoms in the Fermi sea can be tuned by adjusting the temperature-dependent chemical potential  $\mu(T)$ . We often measure the single-particle energy of atoms from the chemical potential and therefore define  $\xi_{\mathbf{k}} \equiv \epsilon_{\mathbf{k}} - \mu$ . Hereafter, for clarity we will suppress the volume  $V$  in expressions, so the summation over the momentum  $\sum_{\mathbf{k}}$  in the later equations should be understood as  $\sum_{\mathbf{k}} = (1/V) \int d\mathbf{k} / (2\pi)^3$ .

### B. Diagrammatic theory

We use the non-self-consistent many-body  $T$ -matrix theory [28,35] to solve the Fermi-spin-polaron problem, within which the motion of the impurity can be described by a series of ladder diagrams that take into account the successive forward scatterings between the impurity and the atoms in the Fermi bath. By summing up the infinitely many ladder diagrams, as detailed in Appendix, we find the two-particle vertex function, which takes the  $2 \times 2$  matrix form

$$\begin{bmatrix} \Gamma_{11} & \Gamma_{12} \\ \Gamma_{21} & \Gamma_{22} \end{bmatrix} = \begin{bmatrix} 1/g_1 + \tilde{\chi}_{11}(\mathcal{Q}) & \tilde{\chi}_{12}(\mathcal{Q}) \\ \tilde{\chi}_{21}(\mathcal{Q}) & 1/g_2 + \tilde{\chi}_{22}(\mathcal{Q}) \end{bmatrix}^{-1}, \quad (9)$$

where  $\mathcal{Q} \equiv (\mathbf{q}, iv_q)$  is the shorthand notation for the four-dimensional momentum with bosonic Matsubara frequency  $v_q = 2q\pi k_B T$  and integer  $q = 0, \pm 1, \pm 2, \dots$ , and the various pair propagators  $\tilde{\chi}_{ij}$  ( $i, j = 1, 2$ ) are given by

$$\tilde{\chi}_{ij}(\mathcal{Q}) = \sum_{\mathbf{k}} k_B T \sum_{i\omega_k} \mathcal{G}(\mathcal{K}) G_{ij}^{(0)}(\mathcal{Q} - \mathcal{K}). \quad (10)$$

Here we have introduced  $\mathcal{K} \equiv (\mathbf{k}, i\omega_k)$ , with fermionic Matsubara frequency  $\omega_k = (2k+1)\pi k_B T$  and integer  $k = 0, \pm 1, \pm 2, \dots$ , and

$$\mathcal{G}(\mathcal{K}) = \frac{1}{i\omega_k - \xi_{\mathbf{k}}} = \frac{1}{i\omega_k - \epsilon_{\mathbf{k}} + \mu} \quad (11)$$

is the thermal Green's function for noninteracting fermionic atoms in the Fermi bath. The summation over the fermionic

Matsubara frequency in Eq. (10) is easy to carry out. In the single impurity limit, we find that [35]

$$\tilde{\chi}_{11} = \sum_{\mathbf{k}} \left( \frac{v^2[f(\xi_{\mathbf{k}}) - 1]}{i\nu_q - E_{\mathbf{q}-\mathbf{k}}^{(+)} - \xi_{\mathbf{k}}} + \frac{u^2[f(\xi_{\mathbf{k}}) - 1]}{i\nu_q - E_{\mathbf{q}-\mathbf{k}}^{(-)} - \xi_{\mathbf{k}}} \right), \quad (12)$$

$$\tilde{\chi}_{12} = \sum_{\mathbf{k}} \left( \frac{uv[f(\xi_{\mathbf{k}}) - 1]}{i\nu_q - E_{\mathbf{q}-\mathbf{k}}^{(+)} - \xi_{\mathbf{k}}} - \frac{uv[f(\xi_{\mathbf{k}}) - 1]}{i\nu_q - E_{\mathbf{q}-\mathbf{k}}^{(-)} - \xi_{\mathbf{k}}} \right), \quad (13)$$

$\tilde{\chi}_{21} = \tilde{\chi}_{12}$ , and  $\tilde{\chi}_{22}$  can be obtained from  $\tilde{\chi}_{11}$  by exchanging the factor  $u^2$  with  $v^2$  in the large parentheses. The function  $f(x) = 1/(e^{x/k_B T} + 1)$  is the Fermi-Dirac distribution at temperature  $T$ . It is readily seen that the integral in both  $\tilde{\chi}_{11}$  and  $\tilde{\chi}_{22}$  has an ultraviolet divergence at large momentum. This divergence is due to the use of the  $s$ -wave contact interactions and can be exactly compensated by the counterterm in the regularization relation (8), i.e.,  $\sum_{\mathbf{k}} 2m_r/\hbar^2 \mathbf{k}^2$ . Therefore, it is convenient to introduce  $\chi_{11} \equiv 1/g_1 + \tilde{\chi}_{11}$  and  $\chi_{22} \equiv 1/g_2 + \tilde{\chi}_{22}$  and rewrite  $\chi_{12} \equiv \tilde{\chi}_{12}$  and  $\chi_{21} \equiv \tilde{\chi}_{21}$ . We will still refer to  $\chi_{ij}(\mathcal{Q})$  as the pair propagators, without any confusion.

The integrals in  $\chi_{ij}(\mathcal{Q})$  can be categorized into two types [35]. The first is the two-body part, which can be analytically evaluated by using

$$\sum_{\mathbf{k}} \left( \frac{1}{\Omega - \epsilon_{\mathbf{q}-\mathbf{k}}^{(l)} - \xi_{\mathbf{k}}} + \frac{2m_r}{\hbar^2 \mathbf{k}^2} \right) = -\frac{i(2m_r)^{3/2} \sqrt{\Omega - \zeta_{\mathbf{q}}}}{4\pi \hbar^3} \quad (14)$$

for any complex frequency  $\Omega$ . Here  $\zeta_{\mathbf{q}} \equiv \hbar^2 \mathbf{q}^2 / 2(m + m_I) - \mu$  is the center-of-mass kinetic energy measured from the chemical potential. Another is the many-body part, which takes the form

$$\chi_{\text{eff}}(\mathbf{q}, \Omega) = \sum_{\mathbf{k}} \frac{f(\xi_{\mathbf{k}})}{\Omega - \epsilon_{\mathbf{q}-\mathbf{k}}^{(l)} - \xi_{\mathbf{k}}} \quad (15)$$

and can be numerically calculated in a very efficient way, as discussed in detail in our recent work (see, e.g., Appendix A of Ref. [35]). By defining two constants  $\gamma_{\pm} = (\Delta \pm \sqrt{\Delta^2 + \Omega^2})/2$  and rewriting  $E_{\mathbf{p}}^{(\pm)} = \epsilon_{\mathbf{p}}^{(l)} + \gamma_{\pm}$ , it is then easy to check that  $[\mathcal{Q} = (\mathbf{q}, i\nu_q) \equiv (\mathbf{q}, \Omega)]$

$$\begin{aligned} \chi_{11}(\mathcal{Q}) &= \frac{m_r}{2\pi \hbar^2 a_1} + \frac{im_r^{3/2}}{\sqrt{2\pi} \hbar^3} (v^2 \sqrt{\Omega - \gamma_+ - \zeta_{\mathbf{q}}} \\ &\quad + u^2 \sqrt{\Omega - \gamma_- - \zeta_{\mathbf{q}}} + v^2 \chi_{\text{eff}}(\mathbf{q}, \Omega - \gamma_+) \\ &\quad + u^2 \chi_{\text{eff}}(\mathbf{q}, \Omega - \gamma_-), \end{aligned} \quad (16)$$

$$\begin{aligned} \chi_{12}(\mathcal{Q}) &= \frac{im_r^{3/2}}{\sqrt{2\pi} \hbar^3} uv (\sqrt{\Omega - \gamma_+ - \zeta_{\mathbf{q}}} - \sqrt{\Omega - \gamma_- - \zeta_{\mathbf{q}}}) \\ &\quad + uv [\chi_{\text{eff}}(\mathbf{q}, \Omega - \gamma_+) - \chi_{\text{eff}}(\mathbf{q}, \Omega - \gamma_-)], \end{aligned} \quad (17)$$

$$\begin{aligned} \chi_{22}(\mathcal{Q}) &= \frac{m_r}{2\pi \hbar^2 a_2} + \frac{im_r^{3/2}}{\sqrt{2\pi} \hbar^3} (u^2 \sqrt{\Omega - \gamma_+ - \zeta_{\mathbf{q}}} \\ &\quad + v^2 \sqrt{\Omega - \gamma_- - \zeta_{\mathbf{q}}} + u^2 \chi_{\text{eff}}(\mathbf{q}, \Omega - \gamma_+) \\ &\quad + v^2 \chi_{\text{eff}}(\mathbf{q}, \Omega - \gamma_-). \end{aligned} \quad (18)$$

Here, for later convenience of taking analytic continuation (i.e.,  $i\nu_q \rightarrow \Omega + i0^+$ ), we have explicitly set  $i\nu_q = \Omega$ . The

analytic continuation can then be performed by simply adding  $i0^+$  to  $\Omega$ .

Once the pair propagators  $\chi_{ij}(\mathcal{Q})$  are obtained, we take the matrix inverse to find the  $2 \times 2$  vertex function  $\Gamma(\mathcal{Q}) = [\chi(\mathcal{Q})]^{-1}$ . The  $2 \times 2$  self-energy of the impurity  $\Sigma_{ij}(\mathcal{P})$  can be obtained by winding back the outgoing leg of the fermionic field operator in the vertex function  $\Gamma(\mathcal{Q})_{ij}$  and by connecting it with the incoming leg of the fermionic field operator [28,35]. Physically, this describes the single particle-hole excitation across the Fermi surface of the bath [28,34,37]. Thus, we have

$$\Sigma_{ij}(\mathcal{P}) = \sum_{\mathbf{q}} k_B T \sum_{i\nu_q} \Gamma_{ij}(\mathcal{Q}) \frac{1}{i\nu_q - i\omega_p - \xi_{\mathbf{q}-\mathbf{p}}}. \quad (19)$$

The summation over the bosonic Matsubara frequency  $\nu_q = 2q\pi k_B T$  (with integer  $q = 0, \pm 1, \pm 2, \dots$ ) can be easily carried out, leading to [28,35]

$$\Sigma_{ij}(\mathbf{p}, i\omega_p) = \sum_{\mathbf{q}} f(\xi_{\mathbf{q}-\mathbf{p}}) \Gamma_{ij}(\mathbf{q}, i\omega_p + \xi_{\mathbf{q}-\mathbf{p}}). \quad (20)$$

### C. Analytic continuation and numerical calculations

We are interested in the retarded impurity Green's functions given by the Dyson equation

$$\mathbf{G}(\mathbf{p}, \omega) = [\mathbf{G}_0^{-1}(\mathbf{p}, \omega) - \mathbf{\Sigma}(\mathbf{p}, \omega)]^{-1} \quad (21)$$

and the related impurity spectral functions  $\mathbf{A}(\mathbf{p}, \omega)$ ,

$$\begin{bmatrix} A_{11} & A_{12} \\ A_{21} & A_{22} \end{bmatrix} = -\frac{1}{\pi} \text{Im} \begin{bmatrix} G_{11}(\mathbf{p}, \omega) & G_{12}(\mathbf{p}, \omega) \\ G_{21}(\mathbf{p}, \omega) & G_{22}(\mathbf{p}, \omega) \end{bmatrix}. \quad (22)$$

Here  $\mathbf{G}_0(\mathbf{p}, \omega)$  and  $\mathbf{\Sigma}(\mathbf{p}, \omega)$  are given by Eqs. (6) and (20), respectively, with the analytic continuation (i.e.,  $i\omega_p \rightarrow \omega + i0^+$ ) explicitly performed. As mentioned earlier, this analytic continuation can be trivially done by replacing  $\Omega$  in Eqs. (16)–(18) with  $\Omega + i0^+$  for the calculations of the retarded pair propagators  $\chi_{ij}(\mathbf{q}, \Omega)$ . The consequent matrix inverse leads to the retarded two-particle vertex functions  $\Gamma_{ij}(\mathbf{q}, \Omega)$ , which is to be used in Eq. (20).

In our numerical calculations, we take the Fermi wave vector  $k_F \equiv (6\pi^2 n)^{1/3}$  and Fermi energy  $\varepsilon_F \equiv \hbar^2 k_F^2 / 2m$  as the units of the momentum (or wave vector) and energy, respectively. The temperature  $T$  is accordingly measured in units of the Fermi temperature  $T_F = \varepsilon_F / k_B$ . The choice of this natural unit amounts to setting  $2m = \hbar = k_B = 1$ . As we take the equal mass for the impurity and background fermionic atoms ( $m = m_I$ ), the reduced mass  $m_r = \frac{1}{4}$ . In Eqs. (16)–(18) we find that  $m_r / 2\pi \hbar^2 a_i = 1/8\pi a_i$  ( $i = 1, 2$ ),  $m_r^{3/2} / \sqrt{2\pi} \hbar^3 = 1/8\sqrt{2}\pi$ , and  $\zeta_{\mathbf{q}} = \mathbf{q}^2 / 2 - \mu$ . The dimensionless expression of  $\chi_{\text{eff}}(\mathbf{q}, \Omega + i0^+)$  can be found in Appendix A of Ref. [35].

## III. QUASIPARTICLE PROPERTIES OF FERMI SPIN POLARONS

In the experiments on dissipative Rabi dynamics [13,15,18], the interaction between the spin-down impurity and the Fermi bath ( $a_{\downarrow}$  or  $a_2$ ) is typically small. For convenience, we simply set  $a_2 = 0^-$  and define  $a_{\uparrow} = a_1 = a$ . Therefore, in Eq. (18)  $\chi_{22}(\mathcal{Q}) \rightarrow \infty$ . By taking the matrix inverse, only the 11 component of the matrices, such as

the two-particle vertex function  $\Gamma_{11}(\mathcal{Q}) = \chi_{11}^{-1}(\mathcal{Q})$  and the self-energy  $\Sigma_{11}(\mathbf{p}, \omega)$ , is nonzero. We note that the case with a small but positive scattering length  $a_2 > 0$  might be useful to understand the residual final-state effect in the rf spectroscopy [11,16] or Raman spectroscopy [19] and could be addressed in future studies.

### A. Self-energy

For the case of  $a_2 = 0$ , it is useful to contrast our  $T$ -matrix result (21) with another approximated impurity Green's function [18,26]

$$\mathbf{G}(\mathbf{p}, \omega) = \begin{bmatrix} \omega - \epsilon_{\mathbf{p}}^{(I)} - \Sigma^{(0)}(\mathbf{p}, \omega) & -\Omega/2 \\ -\Omega/2 & \omega - \epsilon_{\mathbf{p}}^{(I)} - \Delta \end{bmatrix}^{-1}, \quad (23)$$

where  $\Sigma^{(0)}(\mathbf{p}, \omega)$  is the impurity self-energy of the spin-up state, determined in the absence of the Rabi coupling. Thus, the impurity Green's function  $G(\mathbf{p}, \omega) = 1/[\omega - \epsilon_{\mathbf{p}}^{(I)} - \Sigma^{(0)}(\mathbf{p}, \omega)]$  describes a Fermi polaron when the impurity is always kept to the spin-up state. Earlier pioneering investigations of the dissipative Fermi-polaron Rabi dynamics [25,26] rely on the applicability of Eq. (23), which is justified in the limit of small Rabi couplings (i.e.,  $\Omega \rightarrow 0$ ), where the correction arising from the Rabi coupling to the self-energy  $\Sigma^{(0)}(\mathbf{p}, \omega)$  would scale like  $(\Omega/\varepsilon_F)^2$ . However, in the experiments [13,15,18], typically a reasonably large Rabi coupling  $\Omega \sim 0.7\varepsilon_F$  has to be taken, in order to have measurable signals. The validity of Eq. (23) for these Rabi coupling strengths (i.e.,  $\Omega \sim \varepsilon_F$ ) then should be carefully examined.

The  $T$ -matrix result (21) is useful to check such a validity, as the self-energy  $\Sigma_{11}(\mathbf{p}, \omega)$  is obtained in the presence of the Rabi coupling. In Figs. 1 and 2 we show the zero-momentum impurity self-energy  $\Sigma_{11}(\mathbf{p} = \mathbf{0}, \omega)$  at different Rabi coupling strengths, in the unitary limit ( $a = \pm\infty$ ) and at the interaction strength  $1/k_F a = 0.5$ , respectively. For these two cases, we focus on the attractive and repulsive polaron branches, respectively, by choosing the detuning  $\Delta = E_{\text{att}}$  and  $\Delta = E_{\text{rep}}$ , where the energies of both attractive ( $E_{\text{att}}$ ) and repulsive polarons ( $E_{\text{rep}}$ ) are determined without the Rabi coupling [35].

For the very small Rabi coupling  $\Omega = 0.1\varepsilon_F$ , the self-energy  $\Sigma_{11}(\mathbf{p}, \omega)$  is essentially  $\Sigma^{(0)}(\mathbf{p}, \omega)$ . By increasing  $\Omega$  to  $\varepsilon_F$ , we can see a quantitative modification to the self-energy. Although this modification is noticeable, it still seems to be small enough to validate the approximate impurity Green's function in Eq. (23). At the large Rabi coupling  $\Omega = 2\varepsilon_F$ , there are qualitative changes to the self-energy, as indicated by the large shifts in the local minimum and/or maximum positions in both  $\text{Re}\Sigma_{11}(\mathbf{0}, \omega)$  and  $\text{Im}\Sigma_{11}(\mathbf{0}, \omega)$ .

These changes indicate that, under the strong driving condition with  $\Omega \gg \varepsilon_F$ , the quasiparticle properties of Fermi polarons are strongly modified. Therefore, in the Rabi oscillation experiments, we can no longer probe the polaron physics without Rabi coupling, which is determined by the self-energy  $\Sigma^{(0)}(\mathbf{p}, \omega)$  at  $\Omega = 0$ . In more detail, through strongly driven Rabi oscillations, we would instead measure  $\Omega$ -dependent attractive and repulsive polaron energies and their  $\Omega$ -dependent decay rates. The decay rate is roughly proportional to  $-\text{Im}\Sigma_{11}(\mathbf{0}, \omega)$ . As indicated by the arrows in Figs. 1(b) and 2(b), we find that the imaginary part of

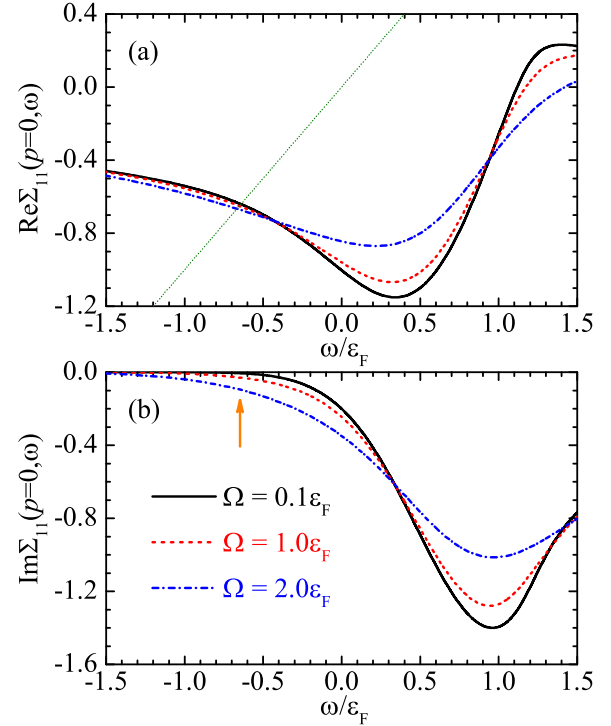


FIG. 1. (a) Real part and (b) imaginary part of the impurity self-energy  $\Sigma_{11}(\mathbf{p}, \omega)$  at zero momentum ( $\mathbf{p} = \mathbf{0}$ ) in the unitary limit  $1/a = 0$  at the interaction strength  $1/k_F a = 0$ . The self-energy is in units of  $\varepsilon_F$ , where  $\varepsilon_F \equiv \hbar^2 k_F^2 / 2m$  and  $k_F = (6\pi^2 n)^{1/3}$  are the Fermi energy and Fermi wave vector, respectively. The temperature is  $T = 0.2T_F = 0.2\varepsilon_F/k_B$  and the detuning is equal to the attractive polaron energy (at zero Rabi coupling)  $\Delta = E_{\text{att}}$ . We consider three characteristic Rabi couplings  $\Omega = 0.1\varepsilon_F$  (black solid line),  $1.0\varepsilon_F$  (red dashed line), and  $2.0\varepsilon_F$  (blue dot-dashed line). The green dotted line in (a) shows the curve  $y = \omega$ . The arrow in (b) points to the attractive polaron energy  $E_{\text{att}} \simeq -0.64\varepsilon_F$ .

the self-energy  $-\text{Im}\Sigma_{11}(\mathbf{0}, \omega)$  increases with increasing Rabi coupling strength. The change in  $-\text{Im}\Sigma_{11}(\mathbf{0}, \omega \sim E_{\text{att}})$  of the attractive polaron branch is particularly significant at large Rabi coupling: It increases from a negligible value  $0.006\varepsilon_F$  to a considerable value  $0.097\varepsilon_F$ . As we will see, this will bring an additional damping to Fermi-polaron Rabi oscillations.

### B. Single-particle spectral function

Using the self-energy  $\Sigma_{11}(\mathbf{p}, \omega)$  in Eq. (21), we calculate directly the impurity Green's functions  $G_{11}(\mathbf{p}, \omega)$  and  $G_{22}(\mathbf{p}, \omega)$  and the associated single-particle spectral functions  $A_{11}(\mathbf{p}, \omega)$  and  $A_{22}(\mathbf{p}, \omega)$ . Two example cases of the zero-momentum spectral function are shown in Figs. 3 and 4 for the interaction strengths  $1/k_F a = 0$  and  $0.5$ , respectively. In each case, we consider the resonant detuning for attractive or repulsive polarons.

It is readily seen that there are several peaks in the spectral functions  $A_{11}(\mathbf{0}, \omega)$  and  $A_{22}(\mathbf{0}, \omega)$ . Each peak corresponds to a well-defined quasiparticle, with its lifetime characterized by the width of the peak. To determine the peak positions or the quasiparticle energies, it is useful to approximate the impurity

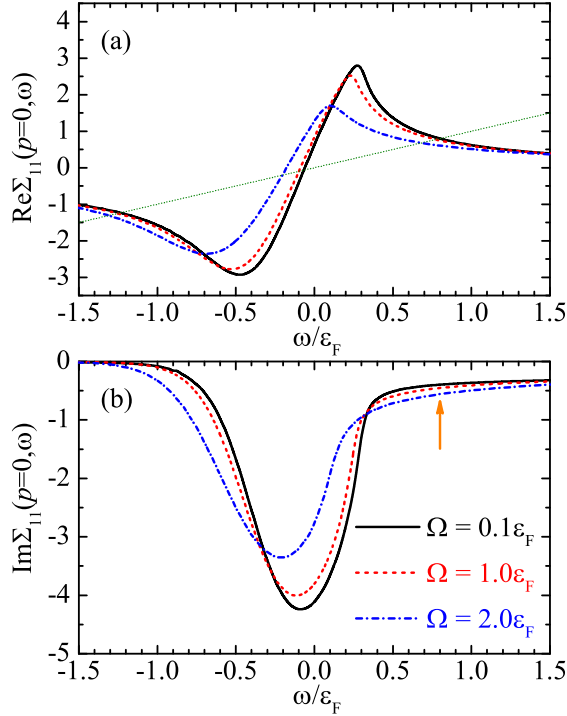


FIG. 2. (a) Real part and (b) imaginary part of the impurity self-energy  $\Sigma_{11}(\mathbf{p}, \omega)$  at zero momentum ( $\mathbf{p} = \mathbf{0}$ ) at the interaction strength  $1/k_F a = 0.5$ . The self-energy is in units of  $\varepsilon_F$ . The temperature is  $T = 0.2T_F$  and the detuning is equal to the repulsive polaron energy (at zero Rabi coupling)  $\Delta = E_{\text{rep}}$ . We consider three characteristic Rabi couplings  $\Omega = 0.1\varepsilon_F$  (black solid line),  $1.0\varepsilon_F$  (red dashed line), and  $2.0\varepsilon_F$  (blue dot-dashed line). The green dotted line in (a) shows the curve  $y = \omega$ . The arrow in (b) points to the repulsive polaron energy  $E_{\text{rep}} \simeq 0.80\varepsilon_F$ .

Green's function in Eq. (21) at zero momentum  $\mathbf{p} = 0$  as [18]

$$\mathbf{G}(\mathbf{0}, \omega) = \begin{bmatrix} \mathcal{Z}^{-1}(\omega - \mathcal{E}_P + i\Gamma/2) & -\Omega/2 \\ -\Omega/2 & \omega - \Delta \end{bmatrix}^{-1}. \quad (24)$$

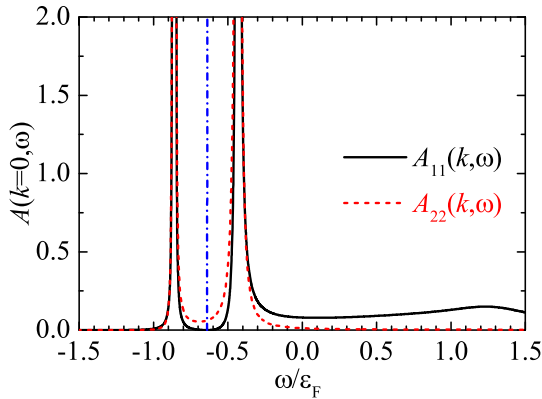


FIG. 3. Zero-momentum impurity spectral functions  $A_{11}(\mathbf{p} = \mathbf{0}, \omega)$  and  $A_{22}(\mathbf{p} = \mathbf{0}, \omega)$  in the unitary limit  $1/a = 0$  at the detuning  $\Delta = E_{\text{att}}$ . The impurity spectral function is in units of  $\varepsilon_F^{-1}$ . The temperature is  $T = 0.2T_F$  and the Rabi coupling is  $\Omega = 0.5\varepsilon_F$ . The blue dot-dashed line indicates the peak position  $\omega_p = E_{\text{att}} \simeq -0.64\varepsilon_F$  of the impurity spectral function without Rabi coupling  $\Omega = 0$ .

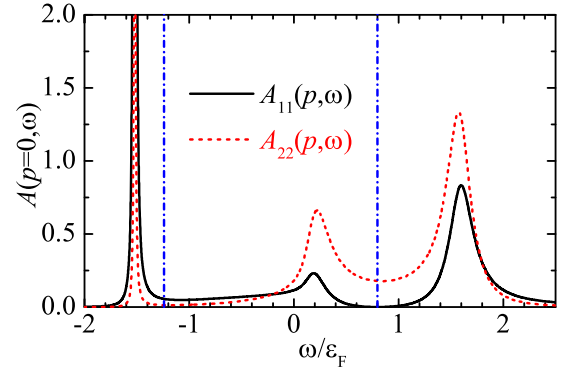


FIG. 4. Zero-momentum impurity spectral functions  $A_{11}(\mathbf{p} = \mathbf{0}, \omega)$  and  $A_{22}(\mathbf{p} = \mathbf{0}, \omega)$  at the interaction strength  $1/k_F a = 0.5$  at the detuning  $\Delta = E_{\text{rep}}$ . The impurity spectral function is in units of  $\varepsilon_F^{-1}$ . The temperature is  $T = 0.2T_F$  and the Rabi coupling is  $\Omega = 2.0\varepsilon_F$ . The blue dot-dashed line on the right indicates the peak position  $\omega_p = E_{\text{rep}} \simeq +0.80\varepsilon_F$  of the impurity spectral functions  $A_{11}$  and  $A_{22}$  without Rabi coupling  $\Omega = 0$ . We note that the impurity spectral function  $A_{11}$  has an additional peak (of the attractive polaron) at  $\omega_p = E_{\text{att}} \simeq -1.24\varepsilon_F$ , as indicated by the blue dot-dashed line on the left.

Here we assume that the Green's function  $[\omega - \varepsilon_{\mathbf{p}}^{(l)} - \Sigma_{11}(\mathbf{p}, \omega)]^{-1}$  describes a Fermi polaron in the spin-up state with zero-momentum polaron energies  $\mathcal{E}_P$  satisfying  $\mathcal{E}_P = \text{Re}\Sigma_{11}(\mathbf{0}, \omega = \mathcal{E}_P)$  and therefore approximate

$$\frac{1}{\omega - \Sigma_{11}(\mathbf{0}, \omega)} \simeq \frac{1}{(\omega - \mathcal{E}_P)(1 - \frac{\partial \text{Re}\Sigma_{11}}{\partial \omega}) - i \text{Im}\Sigma_{11}} \quad (25)$$

by Taylor expanding  $\Sigma_{11}(\mathbf{0}, \omega)$  near  $\omega = \mathcal{E}_P$ . Following the standard way [28,35] to introduce the residue  $\mathcal{Z} = (1 - \partial \text{Re}\Sigma_{11}/\partial \omega)^{-1}$  and decay rate  $\Gamma = -2\mathcal{Z} \text{Im}\Sigma_{11}$ , we then arrive at Eq. (24). This approximate form of the impurity Green's function is very useful to understand the Rabi dynamics of the Fermi polaron in the spin-up state, as suggested in Ref. [18]. For example, at the resonant detuning  $\Delta = \mathcal{E}_P$ , it is easy to find that the poles of Eq. (24) satisfy the equation

$$\left(E - \mathcal{E}_P + i\frac{\Gamma}{2}\right)(E - \mathcal{E}_P) - \mathcal{Z}\frac{\Omega^2}{4} = 0 \quad (26)$$

and are given by  $(\Gamma_R \equiv \Gamma/2)$  [18,27]

$$E_{\pm} = \left(\mathcal{E}_P \pm \frac{1}{2}\sqrt{\mathcal{Z}\Omega^2 - \Gamma_R^2}\right) - i\frac{\Gamma_R}{2}. \quad (27)$$

The form of the quasiparticle energies in the above equation clearly indicates Rabi oscillations with a modified effective Rabi coupling strength  $\Omega_{\text{eff}} = \sqrt{\mathcal{Z}}\Omega$  and with a damping rate  $\Gamma_R = \Gamma/2$ . Therefore, if one neglects the  $\Omega$  dependence of the residue  $\mathcal{Z}$  and of the decay rate  $\Gamma$  (which seems justified from Figs. 1 and 2 for  $\Omega < \varepsilon_F$ , as we have discussed in the preceding section), one can directly extract both the residue and decay rate of Fermi polarons from Rabi oscillations [13,15,18]. In the strong driving regime  $\Omega \gg \varepsilon_F$  instead we anticipate that the effective Rabi coupling strength  $\Omega_{\text{eff}}$  will deviate from  $\sqrt{\mathcal{Z}}\Omega$ . Further discussion of this point will be provided in the next section.

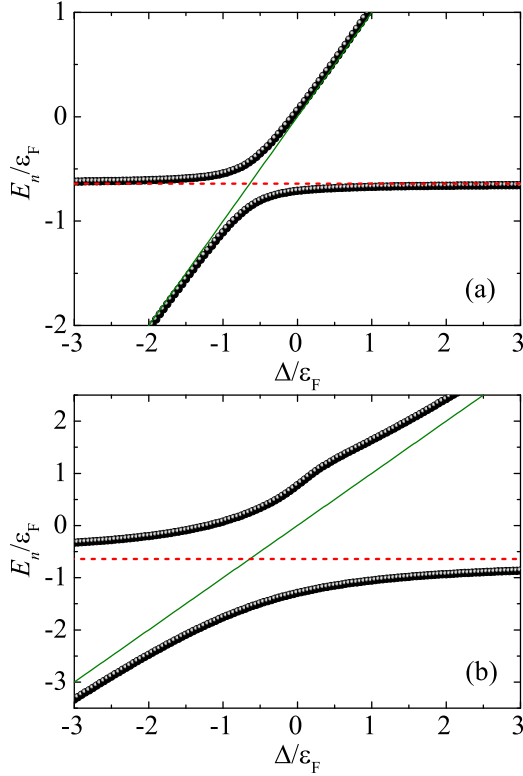


FIG. 5. Zero-momentum energies of Fermi spin polarons as a function of the detuning  $\Delta$  in the unitary limit  $1/a$ , at the Rabi frequencies (a)  $\Omega = 0.5\varepsilon_F$  and (b)  $\Omega = 2.0\varepsilon_F$ . The temperature is  $T = 0.2T_F$ . The green solid lines show  $y = \Delta$ , while the horizontal red dashed lines indicate the attractive polaron energy (at zero Rabi coupling)  $E_{\text{att}} \approx -0.64\varepsilon_F$ .

As shown in Fig. 3, for the unitary impurity-bath interaction, where only attractive polaron exists, we find two peaks with position well described by Eq. (27). The situation becomes a little complicated at the interaction strength  $1/k_F a = 0.5$ , as reported in Fig. 4. There we have both an attractive polaron and a repulsive polaron in the spin-up state. As we choose a resonant detuning  $\Delta = \mathcal{E}_P = E_{\text{rep}}$  for the repulsive branch, there are two peaks locating at the positive energy and roughly satisfying Eq. (27). However, there is also a peak at about the attractive polaron energy  $\mathcal{E}_P = E_{\text{att}} \sim -1.24\varepsilon_F$ . This peak is not taken into account in the approximate impurity Green's function (24), but it could be obtained by numerically solving the poles of the full impurity Green's function (21).

### C. Energies of Fermi spin polarons

We have numerically determined the poles of the full impurity Green's function in Eq. (21), by neglecting the imaginary part of the self-energy  $\text{Im}\Sigma_{11}$ . The results in the unitary limit and at  $1/k_F a = 0.5$  as a function of the detuning are shown in Figs. 5 and 6, respectively, at two Rabi coupling strengths  $\Omega = 0.5\varepsilon_F$  [Figs. 5(a) and 6(a)] and  $\Omega = 2\varepsilon_F$  [Figs. 5(b) and 6(b)].

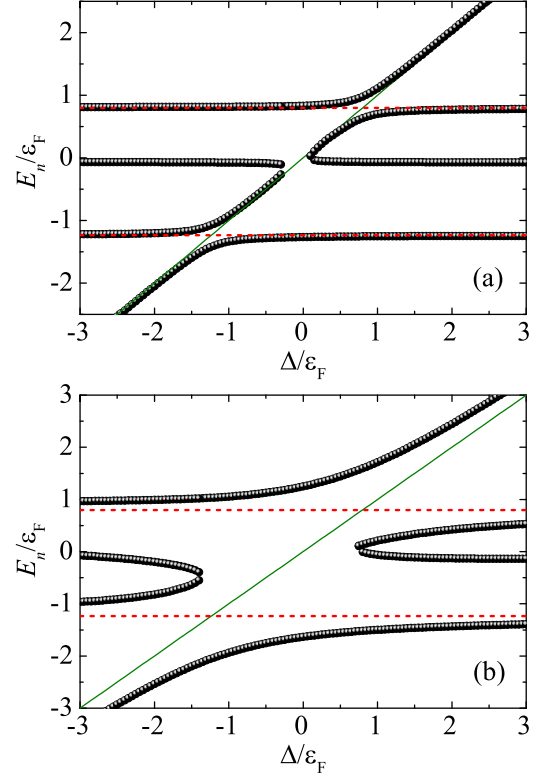


FIG. 6. Zero-momentum energies of Fermi spin polarons as a function of the detuning  $\Delta$  at the interaction strength  $1/k_F a = 0.5$  and at the Rabi frequencies (a)  $\Omega = 0.5\varepsilon_F$  and (b)  $\Omega = 2.0\varepsilon_F$ . The temperature is  $T = 0.2T_F$ . The green solid lines show  $y = \Delta$ . The two horizontal red dashed lines indicate the attractive polaron energy (at zero Rabi coupling)  $E_{\text{att}} \approx -1.24\varepsilon_F$  and the repulsive polaron energy (at zero Rabi coupling)  $E_{\text{rep}} \approx 0.80\varepsilon_F$ .

In the unitary limit (Fig. 5), we find two energies of the Fermi spin polaron, which basically follow

$$E_{\pm} = \frac{1}{2}[\mathcal{E}_P + \Delta \pm \sqrt{Z\Omega^2 - (\mathcal{E}_P - \Delta)^2}] \quad (28)$$

if we neglect the small decay rate (i.e.,  $\Gamma \ll \varepsilon_F$ ). This is particularly evident at the small Rabi coupling [see Fig. 5(a)], where both energies follow  $\mathcal{E}_P$  and  $\Delta$  far off the resonance and exhibit a well-defined avoided crossing at the resonance  $\Delta = \mathcal{E}_P$ . At the large Rabi coupling [Fig. 5(b)], however, we find that the upper branch of the energies seems to develop an additional structure around zero detuning  $\Delta = 0$ . We attribute it to the strongly modified self-energy  $\Sigma_{11}$  at large Rabi coupling.

At the interaction strength  $1/k_F a = 0.5$  (Fig. 6), we typically find four poles in the impurity Green's function (21). The pole closest to  $E = 0$  is a false solution, since we do not include  $\text{Im}\Sigma_{11}$  in finding the poles of Eq. (21). In general,  $\text{Im}\Sigma_{11}$  takes a very large value near zero energy [see, e.g., Fig. 2(b)]. Thus, it is meaningless to treat the near-zero-energy solution as a well-defined quasiparticle. We find two avoided crossings located at the resonances  $\Delta = E_{\text{att}}$  and  $\Delta = E_{\text{rep}}$ . Far off the resonances, the other three poles basically follow the trace of  $\mathcal{E}_P = E_{\text{att}}$ ,  $\mathcal{E}_P = E_{\text{rep}}$  (see the red dotted lines), and  $\Delta$  (thin green line). At large Rabi coupling, the middle pole

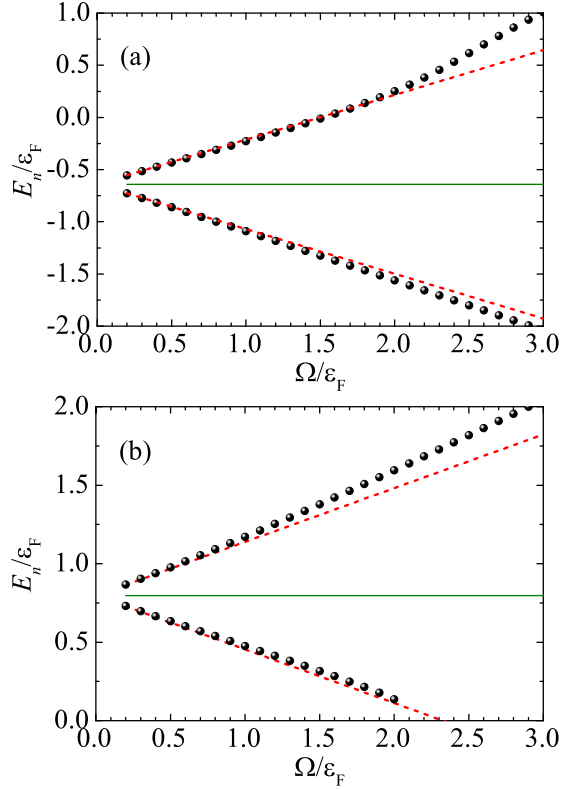


FIG. 7. Zero-momentum energies of Fermi spin polarons as a function of the Rabi coupling  $\Omega$  at the two interaction strengths (a)  $1/k_F a = 0$  and (b)  $1/k_F a = 0.5$ . (a) In the unitary limit  $1/k_F a = 0$ , we take the detuning  $\Delta = E_{\text{att}} \simeq -0.64\epsilon_F$ , while (b) at the interaction strength  $1/k_F a = 0.5$ , we set  $\Delta = E_{\text{rep}} \simeq 0.80\epsilon_F$ . These two detunings are indicated by green solid lines. The red dashed lines show the anticipated energies  $E_n = \Delta \pm \sqrt{\mathcal{Z}}\Omega/2$ , where (a)  $\mathcal{Z}_{\text{att}} \simeq 0.73$  and (b)  $\mathcal{Z}_{\text{rep}} \simeq 0.47$ . The temperature is  $T = 0.2T_F$ .

may disappear at the detuning  $\Delta \sim 0$ , as shown in Fig. 6(b). This is again due to the large value of  $\text{Im}\Sigma_{11}$  near zero energy.

In Fig. 7 we report the energy splitting at the resonant detuning, as a function of the Rabi coupling, as predicted by Eq. (27). By ignoring the small decay rate  $\Gamma_R$ , the energy splitting is given by  $\delta E = \sqrt{\mathcal{Z}}\Omega$ , where  $\mathcal{Z}$  is the residue of either an attractive polaron or a repulsive polaron. For the Rabi coupling  $\Omega \leq \epsilon_F$ , we find that Eq. (27) provides an excellent fit to the numerically extracted quasiparticle energies. At larger Rabi coupling, nonlinear deviation from Eq. (27) becomes sizable, indicating the breakdown of the approximate impurity Green's function in Eq. (24).

#### IV. DISSIPATIVE RABI DYNAMICS OF FERMI POLARONS

Let us now try to better understand the recent experiments on Fermi-polaron Rabi oscillations [13,15,18], by examining more closely the role play by a reasonably large Rabi coupling strength  $\Omega \sim \epsilon_F$ . Experimentally, the impurity is initially prepared in the noninteracting (or weakly interacting) spin-down state. At time zero, a simple square pulse is added to transfer the impurity to the spin-up state that is in strongly interacting with the Fermi bath. The frequency of the pulse is suitably

chosen, so either the attractive polaron branch or the repulsive polaron branch of the spin-up state is selected to be on resonance (i.e.,  $\Delta = E_{\text{att}}$  or  $\Delta = E_{\text{rep}}$ ). After a variable holding time  $t$ , the relative population of the impurity in the spin-down state is then determined.

#### A. Theory of dissipative Rabi oscillation

Physically, for a single impurity this procedure measures the spin-down occupation

$$\begin{aligned} n_{\downarrow}(t) &= \langle \psi(t) | \sum_{\mathbf{p}} d_{\mathbf{p}\downarrow}^{\dagger} d_{\mathbf{p}\downarrow} | \psi(t) \rangle \\ &= \langle \psi(0) | \sum_{\mathbf{p}} d_{\mathbf{p}\downarrow}^{\dagger}(t) d_{\mathbf{p}\downarrow}(t) | \psi(0) \rangle, \end{aligned} \quad (29)$$

where the time-dependent many-body wave function is  $|\psi(t)\rangle = e^{-i\mathcal{H}t/\hbar} |\psi(0)\rangle$ , the time-dependent field operator  $d_{\mathbf{p}\downarrow}(t) = e^{i\mathcal{H}t/\hbar} d_{\mathbf{p}\downarrow} e^{-i\mathcal{H}t/\hbar}$ , and the initial wave function at time  $t = 0$  is given by

$$|\psi(0)\rangle = |\downarrow\rangle_T \otimes |\text{FS}\rangle. \quad (30)$$

Here, since the initial spin-down impurity does not interact with the thermal Fermi bath, we have taken  $|\psi(0)\rangle$  as a direct product of a thermal impurity state  $|\downarrow\rangle_T$  and a thermal Fermi sea  $|\text{FS}\rangle$ . In the Fermi sea, at finite temperature  $T$  fermionic atoms occupy single-particle states according to the Fermi-Dirac distribution. For a single impurity, the thermal probability of the spin-down impurity would be given by a suitable distribution function  $f_{\mathbf{k}}$  that is determined by the type or statistics of the impurity, if it has a momentum  $\mathbf{k}$ . By substituting Eq. (30) into Eq. (29), we find that

$$n_{\downarrow}(t) = \sum_{\mathbf{p}\mathbf{k}} f_{\mathbf{k}} \langle \text{FS} | d_{\mathbf{k}\downarrow} d_{\mathbf{p}\downarrow}^{\dagger}(t) d_{\mathbf{p}\downarrow}(t) d_{\mathbf{k}\downarrow}^{\dagger} | \text{FS} \rangle. \quad (31)$$

It is difficult to exactly evaluate  $n_{\downarrow}(t)$  for long times, which involves a product of four field operators. This is because the effects due to strong correlations will gradually accumulate during the time evolution. For the timescale in the Rabi dynamics experiments (i.e., for a few Rabi oscillations), however, it might be instructive to consider the first-order mean-field-type decoupling

$$\begin{aligned} n_{\downarrow}(t) &\simeq \sum_{\mathbf{p}} f_{\mathbf{p}} \langle d_{\mathbf{p}\downarrow} d_{\mathbf{p}\downarrow}^{\dagger}(t) \rangle \langle d_{\mathbf{p}\downarrow}(t) d_{\mathbf{p}\downarrow}^{\dagger} \rangle \\ &= \sum_{\mathbf{p}} f_{\mathbf{p}} \mathcal{S}_{\downarrow\downarrow}(\mathbf{p}, -t) \mathcal{S}_{\downarrow\downarrow}(\mathbf{p}, t), \end{aligned} \quad (32)$$

as inspired by the well-known Wick theorem in the diagrammatic theory. Here, in the second line we have introduced, for  $t > 0$ ,

$$\mathcal{S}_{\downarrow\downarrow}(\mathbf{p}, t) \equiv \langle \text{FS} | d_{\mathbf{p}\downarrow}(t) d_{\mathbf{p}\downarrow}^{\dagger} | \text{FS} \rangle \equiv \langle d_{\mathbf{p}\downarrow}(t) d_{\mathbf{p}\downarrow}^{\dagger} \rangle. \quad (33)$$

It is easy to recognize that  $\mathcal{S}_{\downarrow\downarrow}(\mathbf{p}, t) = iG_{22}(\mathbf{p}, t)$  is exactly the impurity Green's function in the spin-down channel in the time domain. Therefore, we can determine it directly from the single-particle spectral functions, i.e.,

$$\mathcal{S}_{\downarrow\downarrow}(\mathbf{p}, t) = \int_{-\infty}^{+\infty} d\omega A_{22}(\mathbf{p}, \omega) e^{-i\omega t}, \quad (34)$$

and consequently we are able to calculate

$$n_{\downarrow}(t) \simeq \sum_{\mathbf{p}} f_{\mathbf{p}} |\mathcal{S}_{\downarrow}(\mathbf{p}, t)|^2. \quad (35)$$

An expression similar to Eq. (35) but without the thermal average has been advised by Adlong *et al.* [see Eq. (S46) in the Supplemental Material of Ref. [27]], based on Chevy's variational ansatz.

To show the usefulness of Eq. (35), let us derive an analytic expression of  $n_{\downarrow}(t)$  following Ref. [27], by using the approximate impurity Green's function in Eq. (24) at zero momentum. It is readily seen that the spin-down impurity Green's function then takes the approximate form

$$G_{22}(\mathbf{0}, \omega) = \frac{A}{\omega - E_+ + i\Gamma_R/2} + \frac{1 - A}{\omega - E_- + i\Gamma_R/2}, \quad (36)$$

where the pole energies  $E_+$  and  $E_-$  are given by Eq. (28) and  $A \equiv \frac{1}{2} - (\mathcal{E}_P - \Delta)/2\Omega_{\text{eff}}$  with  $\Omega_{\text{eff}} = \sqrt{\mathcal{Z}\Omega^2 + (\mathcal{E}_P - \Delta)^2}$ . After some straightforward algebra, we find that

$$|\mathcal{S}_{\downarrow}|^2 \simeq e^{-\Gamma_R t} \left( \cos^2 \frac{\Omega_{\text{eff}} t}{2} + \frac{(\mathcal{E}_P - \Delta)^2}{\Omega_{\text{eff}}^2} \sin^2 \frac{\Omega_{\text{eff}} t}{2} \right), \quad (37)$$

which clearly exhibits an oscillation with periodicity  $2\pi/\Omega_{\text{eff}}$  and damping rate  $\Gamma_R$ .

Equations (37) and (35) are not applicable for long evolution times. This is partly reflected in the exponential decay of  $|\mathcal{S}_{\downarrow}|^2$ , which implies that  $n_{\downarrow}(t \rightarrow \infty) = 0$  for any detuning  $\Delta$ . However, at the resonant detuning  $\Delta = \mathcal{E}_P$ , the effective bias for the impurity spin would be zero [24]. Therefore, we should anticipate a zero steady-state magnetization, or  $n_{\uparrow}(t \rightarrow \infty) = n_{\downarrow}(t \rightarrow \infty) = \frac{1}{2}$  [24]. A possible reason why Eq. (35) cannot give a zero steady-state magnetization is that the single impurity condition, i.e.,  $\sum_{\mathbf{p}} [d_{\mathbf{p}\uparrow}^{\dagger}(t)d_{\mathbf{p}\uparrow}(t) + d_{\mathbf{p}\downarrow}^{\dagger}(t)d_{\mathbf{p}\downarrow}(t)] = 1$ , is not strictly satisfied by our approximated mean-field-type decoupling.

To rectify this weakness, it is useful to consider the operator for the spin-down occupation

$$\hat{n}_{\downarrow}(t) = \frac{1}{2} - \frac{1}{2} \sum_{\mathbf{p}} [d_{\mathbf{p}\uparrow}^{\dagger}(t)d_{\mathbf{p}\uparrow}(t) - d_{\mathbf{p}\downarrow}^{\dagger}(t)d_{\mathbf{p}\downarrow}(t)] \quad (38)$$

and then calculate

$$n_{\downarrow}(t) = \sum_{\mathbf{k}} f_{\mathbf{k}} \langle \text{FS} | d_{\mathbf{k}\downarrow} \hat{n}_{\downarrow}(t) d_{\mathbf{k}\downarrow}^{\dagger} | \text{FS} \rangle. \quad (39)$$

By using the mean-field decoupling and repeating the steps that lead to Eq. (35), it is easy to derive that

$$n_{\downarrow}(t) \simeq \frac{1}{2} + \frac{1}{2} \sum_{\mathbf{p}} f_{\mathbf{p}} [|\mathcal{S}_{\downarrow}(\mathbf{p}, t)|^2 - |\mathcal{S}_{\uparrow}(\mathbf{p}, t)|^2], \quad (40)$$

where  $\mathcal{S}_{\uparrow\downarrow}(\mathbf{p}, t)$  takes the form

$$\mathcal{S}_{\uparrow\downarrow}(\mathbf{p}, t) = \int_{-\infty}^{+\infty} d\omega A_{12}(\mathbf{p}, \omega) e^{-i\omega t}. \quad (41)$$

The use of Eq. (40) is still restricted to the short-time evolution of a few Rabi oscillations. However, we anticipate that it may provide a more accurate prediction than Eq. (35) at the resonant detuning, the case that we will focus on.

## B. Comparison between theory and experiments

We consider the recent Rabi oscillation experiment carried out at the European Laboratory for Non-Linear Spectroscopy (LENS) [15]. There, impurities are the minority fermionic  ${}^6\text{Li}$  atoms, initially in the weakly interacting hyperfine state  $|2\rangle$  (i.e., the second-lowest-energy Zeeman state). The impurity concentration is about  $n_{\text{imp}} \simeq 0.15n$ , where  $n$  is the density of the majority  ${}^6\text{Li}$  atoms in the hyperfine state  $|1\rangle$ . The temperature is about  $T \simeq 0.13T_F$ , where the Fermi energy  $T_F$  is determined by the density  $n$ . Therefore, in the Rabi measurement, initially the impurities would follow a Fermi-Dirac distribution of an ideal Fermi gas,  $f_{\mathbf{p}} = f(\epsilon_{\mathbf{p}}^{(I)} - \mu_I)$ , where the impurity chemical potential  $\mu_I$  can be determined by solving the number equation

$$\sum_{\mathbf{p}} f_{\mathbf{p}} = \sum_{\mathbf{p}} \frac{1}{\exp[(\epsilon_{\mathbf{p}}^{(I)} - \mu_I)/k_B T] + 1} = n_{\text{imp}}. \quad (42)$$

Theoretically, we have solved the impurity spectral functions  $A_{12}(\mathbf{p}, \omega)$  and  $A_{22}(\mathbf{p}, \omega)$  at the given experimental Rabi coupling strength  $\Omega \simeq 0.7\epsilon_F$  and at different interaction parameters  $1/k_F a$  and have consequently calculated  $\mathcal{S}_{\uparrow\downarrow}(\mathbf{p}, t)$  and  $\mathcal{S}_{\downarrow}(\mathbf{p}, t)$ . By integrating over the momentum with the distribution function  $f_{\mathbf{p}}$ , we then determine the time dependence of the spin-down occupation  $n_{\downarrow}(t)$  in Eq. (40).

In Fig. 8 we compare our theoretical predictions (lines) with the experimental data (circles) for the repulsive polaron at  $1/k_F a = 1.27$  [Fig. 8(a)] and for the attractive polaron near the unitary limit  $1/k_F a = 0.07$  [Fig. 8(b)] [15]. The red dashed line indicates the result for the zero-momentum polaron, without taking into account the thermal average over the momentum distribution, while the black solid line includes the momentum average at finite temperature. We find good agreement between theory and experiment [15], without any free adjustable parameters. In particular, for the attractive polaron in Fig. 8(b), most of the experimental data are located on the solid line within the experimental error bar. The good agreement partly justifies the approximated mean-field decoupling used to derive Eq. (40) for the short-time evolution of  $n_{\downarrow}(t)$ .

For the repulsive polaron, the agreement also justifies the experimental procedure of extracting the residue of the polaron  $\mathcal{Z}$  from the oscillation periodicity and the effective Rabi coupling strength (i.e.,  $\mathcal{Z} \simeq \Omega_{\text{eff}}^2/\Omega^2$ ) and of measuring the polaron decay rate  $\Gamma$  from the damping of Rabi oscillations (i.e.,  $\Gamma = 2\Gamma_R$ ). However, it should be emphasized that, strictly speaking, the obtained polaron residue and decay rate are not for the zero-momentum polaron at nonzero Rabi coupling, as assumed in the recent theoretical analysis [27] (see, nevertheless, further discussion of the role played by the finite Rabi coupling in Sec. IV D). They are contributed by polarons with different momenta thermally distributed according to  $f_{\mathbf{p}}$ . This is clearly evidenced by the difference between the dashed line and solid line, as shown in Fig. 8(a). Although the difference due to finite momentum is small, it can lead to a quantitative modification to, for example, the theoretically predicted damping for Rabi oscillations.

For the attractive polaron in Fig. 8(b), the difference between the dashed line and solid line is even larger. In



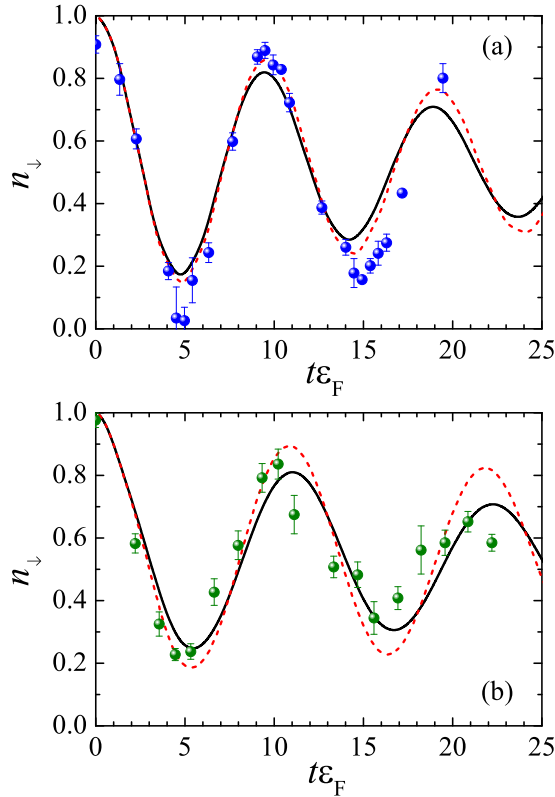


FIG. 8. Comparison of the theory (lines) with the experimental data from the LENS group (symbols) [19], for the Rabi oscillations of (a) a repulsive polaron at  $1/k_F a = 1.27$  and (b) an attractive polaron near the unitary limit  $1/k_F a \simeq 0$ . The data in (a) are extracted from Fig. 2(e) of Ref. [27] and the data in (b) are extracted from Fig. S4(b) of Ref. [15]. For the red dashed lines, we consider the Rabi oscillations of the impurity with zero momentum. For the black solid lines, we include the momentum average, arising from the thermal distribution of the momentum at finite temperature. In the theoretical calculations, we always take the detuning  $\Delta$  that is resonant with either the repulsive polaron energy  $E_{\text{rep}}$  or attractive polaron energy  $E_{\text{att}}$  at zero Rabi coupling. The impurity density is taken as  $n_{\text{imp}}/n = 0.15$ , the Rabi coupling is  $\Omega = 0.7\epsilon_F$ , and the temperature is  $T = 0.13T_F$ , following the experimental conditions [15]. In the comparison, we do not include any adjustable free parameters.

this case, it is worth noting that the damping rate of Rabi oscillations does not correspond to the decay rate of Fermi polarons. Even at zero momentum, the damping rate exhibited by the red dashed line is much larger than the decay rate of the attractive polaron. The latter is actually negligible at  $T = 0.13T_F$  [35]. This inequivalence comes from the fact that the imaginary part of the self-energy  $\text{Im}\Sigma_{11}$  changes dramatically near the attractive polaron energy, as indicated by the arrow in Fig. 1(b). As a result, although the Taylor expansion of  $\text{Re}\Sigma_{11}$  is still meaningful, the expansion of  $\text{Im}\Sigma_{11}$  near the attractive polaron energy becomes problematic for large Rabi coupling. The use of the approximate impurity Green's function (24) then will strongly underestimate the decay rate at the experimental Rabi coupling strength  $\Omega \simeq 0.7\epsilon_F$ . In sharp contrast,  $\text{Im}\Sigma_{11}$  has a very weak energy dependence near the repulsive polaron energy, as seen from Fig. 2(b). The

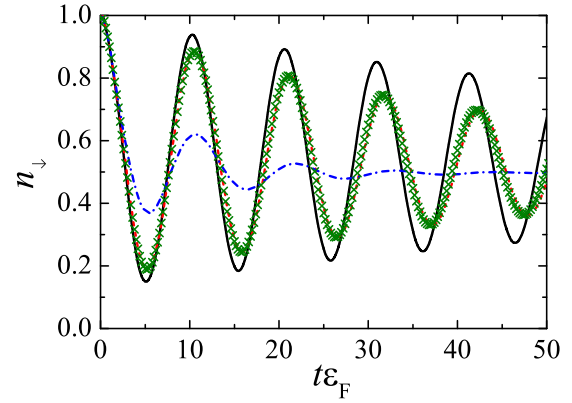


FIG. 9. Rabi oscillations of an attractive polaron in the unitary limit  $1/k_F a = 0$  at different momenta  $k = 0$  (black solid line),  $0.5k_F$  (red dashed line), and  $k_F$  (blue dot-dashed line). The Rabi oscillation after the momentum average is shown by symbols (green crosses). Here the temperature is  $T = 0.1T_F$ , the detuning  $\Delta = E_{\text{att}} \simeq -0.61\epsilon_F$ , and the Rabi coupling  $\Omega = 0.7\epsilon_F$ . For the momentum average, we take the impurity density  $n_{\text{imp}}/n = 0.15$ .

approximate impurity Green's function (24) is an excellent approximation at  $\Omega \simeq 0.7\epsilon_F$  for repulsive Fermi polarons.

### C. Importance of momentum average

Let us now examine more carefully the effect of the momentum average for Rabi oscillations of the attractive polaron. In Fig. 9 we shown the oscillations in  $n_{\downarrow}(t)$  contributed by the momenta  $k = 0$  (black solid line),  $0.5k_F$  (red dashed line), and  $k_F$  (blue dot-dashed line). In comparison to the zero-momentum oscillation, a finite momentum gradually increases the periodicity of Rabi oscillations, in addition to causing more damping. In particular, at large momentum (i.e., the  $k = k_F$  curve), the oscillation becomes overdamped. After taking into account the thermal distribution function  $f_{\mathbf{k}}$ , the final theoretical prediction with momentum average roughly follows the curve at  $0.5k_F$  at the given low temperature  $T = 0.1T_F$ .

### D. Dependence on Rabi coupling

Here we examine the dependence of Rabi oscillations on the Rabi coupling strength. In Figs. 10 and 11 we report the Rabi oscillations of the repulsive and attractive Fermi polarons, respectively, at three Rabi coupling strengths  $\Omega = 0.5\epsilon_F$  (black solid line),  $0.7\epsilon_F$  (red dashed line), and  $\epsilon_F$  (blue dot-dashed line).

For the repulsive polaron at  $1/k_F a = 1$ , the visibility or amplitude of oscillations increases with increasing Rabi coupling, indicating a smaller damping rate. This counterintuitive tendency cannot be simply understood from the picture of a zero-momentum Fermi polaron, whose  $-\text{Im}\Sigma_{11}$  near the repulsive polaron energy would increase with increasing Rabi coupling, as shown in Fig. 2(b). Therefore, the momentum average tends to decrease the damping rate of Rabi oscillations at large Rabi coupling. On the other hand, a finite momentum increases the damping rate at a fixed Rabi coupling, as we already discussed. It is then readily seen that the Rabi coupling

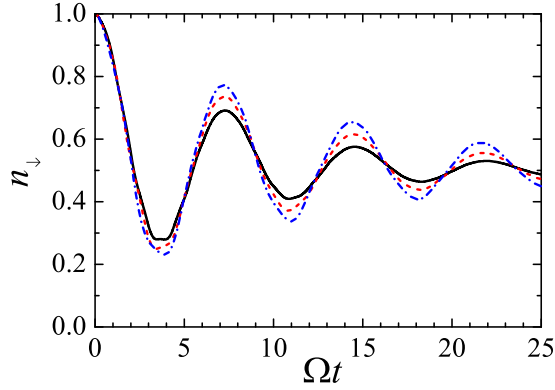


FIG. 10. Momentum-averaged Rabi oscillations of a repulsive polaron at the interaction strength  $1/k_F a = 1$  at different Rabi couplings  $\Omega = 0.5\epsilon_F$  (black solid line),  $0.7\epsilon_F$  (red dashed line), and  $\epsilon_F$  (blue dot-dashed line). Here the temperature is  $T = 0.1T_F$  and the detuning is  $\Delta = E_{\text{rep}} \simeq 0.53\epsilon_F$ . For the momentum average, we take the impurity density  $n_{\text{imp}}/n = 0.15$ .

and finite momentum have opposite effects on the damping of Rabi oscillations. Although these two effects may not completely cancel, it seems reasonable to interpret the observed damping of Rabi oscillation (at finite Rabi coupling with momentum average) as the decay rate of a zero-momentum Fermi polaron (at zero Rabi coupling). This understanding therefore supports the observation found in the LENS experiment [15] that the damping rate of Rabi oscillations quantitatively matches the predicted quasiparticle peak spectral width  $\Gamma$  of repulsive Fermi polarons at zero momentum.

For the attractive polaron in the unitary limit, in contrast, the visibility of Rabi oscillations decreases with increasing Rabi coupling. This enhanced damping can be understood from the rapidly changing  $-\text{Im}\Sigma_{11}$  near the attractive polaron energy, as shown in Fig. 1(b). If we consider the approximated impurity Green's function (24), the effective polaron decay rate is actually given by  $-\text{Im}\Sigma_{11}$  at  $\omega = \epsilon_p + \sqrt{Z}\Omega/2$  [see, e.g., Eq. (27)], which should increase with increasing Rabi coupling. As a result of the additive effects of the momentum

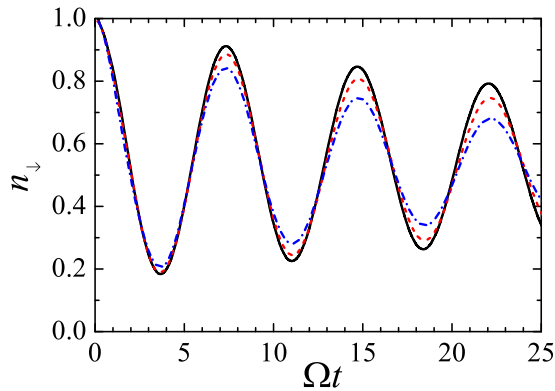


FIG. 11. Momentum-averaged Rabi oscillations of an attractive polaron in the unitary limit  $1/k_F a = 0$  at different Rabi couplings  $\Omega = 0.5\epsilon_F$  (black solid line),  $0.7\epsilon_F$  (red dashed line), and  $\epsilon_F$  (blue dot-dashed line). Here the temperature is  $T = 0.1T_F$  and the detuning is  $\Delta = E_{\text{att}} \simeq -0.61\epsilon_F$ . For the momentum average, we take the impurity density  $n_{\text{imp}}/n = 0.15$ .

average and Rabi coupling on enhancing the damping rate of Rabi oscillations, we conclude that for attractive Fermi polarons, the damping rate of Rabi oscillations cannot be simply interpreted as the zero-momentum quasiparticle decay rate  $\Gamma$ .

We finally note that the periodicity of Rabi oscillations is also slightly affected by a finite Rabi coupling. Large Rabi coupling tends to decrease and increase the periodicity for the repulsive polaron and attractive polaron, respectively. It seems to have the same effect as the momentum average, as shown in Fig. 8. As a result, for repulsive polarons, the combined additive effect of a finite Rabi coupling and momentum average may lead to a smaller periodicity of Rabi oscillations, and hence a larger effective Rabi coupling  $\Omega_{\text{eff}}$ , compared with the expectation from a zero-momentum Fermi polaron, i.e.,  $\sqrt{Z}\Omega$ .

## V. CONCLUSION

In summary, based on the non-self-consistent many-body  $T$ -matrix approximation, we have presented a general theoretical framework of Fermi spin polarons for a spinor impurity immersed in a Fermi bath. We focused on the spin- $\frac{1}{2}$  case with a Rabi coupling  $\Omega$  between the two spin states and addressed the dependence of quasiparticle properties on the Rabi coupling strength. This turns out to be crucial to understand the recent cold-atom experiments on the dissipative Rabi dynamics of Fermi polarons [13,15,18]. In particular, we confirmed that for the Rabi coupling less than the Fermi energy of the Fermi bath, an approximate impurity Green's function provides a reasonable good description of Fermi spin polarons, near the resonant detuning for the repulsive branch.

We then developed an approximate theory for calculating the time evolution of the spin-down occupation, which is measured in the experiments [13,15,18]. This approximate theory relies on a first-order mean-field-type decoupling of a correlation function that involves four field operators, which could be accurate for the short-time evolution. We compared our theoretical predictions on Rabi oscillations with the experimental data [15] and found good agreement without any adjustable free parameters. We analyzed in detail the role played by the momentum average on Rabi oscillations, due to the initial thermal distribution of the impurity at finite temperature. We also addressed the consequence of a finite Rabi coupling at the order of the Fermi energy ( $\Omega \sim \epsilon_F$ ), which could be significant in real experiments. The effects of both factors (i.e., the thermal momentum average and the finite Rabi coupling) were less considered in previous analyses of the dissipative Rabi dynamics [18,27].

We found that, for repulsive polarons, the momentum average and the finite Rabi coupling have opposite effects on the damping of Rabi oscillations. As a result, to a good approximation, we may directly extract the decay rate  $\Gamma$  of a zero-momentum repulsive Fermi polaron at zero Rabi coupling from the damping of Rabi oscillations, a procedure that has already been experimentally adopted [15,18]. For the periodicity of Rabi oscillations, however, the two factors have the same effects: Both of them tend to decrease the periodicity and hence lead to a slightly larger effective Rabi coupling strength than the naive theoretical expectation of  $\sqrt{Z}\Omega$ .

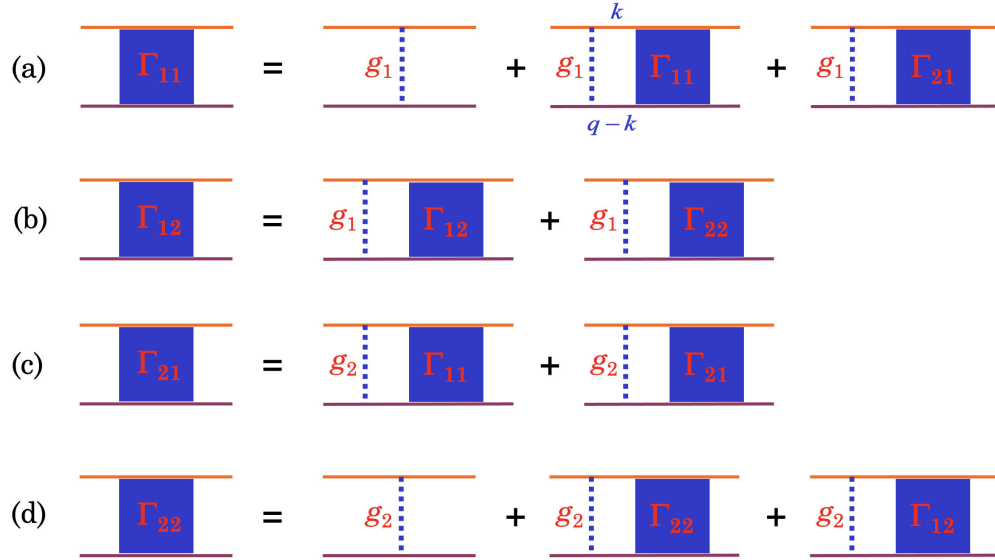


FIG. 12. Diagrammatic representation of the various two-particle vertex functions  $\Gamma_{ij}(Q)$ . Here the upper orange line is the Green's function of fermionic atoms in the bath and the bottom purple line is the impurity Green's function. The dotted lines represent the contact interactions with strengths  $g_i$  ( $i = 1, 2$ ). We do not explicitly label the two hyperfine states of the impurity.

For attractive polarons, on the other hand, the situation turns out to be more complicated. We emphasized that at low temperature, the zero-momentum decay rate of attractive Fermi polarons is not related to the damping of Rabi oscillations. Both the thermal momentum average and the finite Rabi coupling should be carefully taken into account in analyzing the dissipative Rabi dynamics of attractive Fermi polarons.

We finally comment on the theoretical calculation of Rabi oscillations. To go beyond the approximation of the mean-field decoupling, in Eq. (31) we may consider inserting the unity identify between the field operators  $d_{p\downarrow}^\dagger(t)$  and  $d_{p\downarrow}(t)$ ,

$$1 = |\text{FS}\rangle\langle\text{FS}| + \sum_{\mathbf{p},\mathbf{h}} c_{\mathbf{p}}^\dagger c_{\mathbf{h}} |\text{FS}\rangle\langle\text{FS}| c_{\mathbf{h}}^\dagger c_{\mathbf{p}} + \dots, \quad (43)$$

where the second term stands for the many-body state of the Fermi bath with one particle-hole excitation and the ellipsis denotes the many-body states with multiple particle-hole excitations. It is easy to see that the first term in the unity identity  $|\text{FS}\rangle\langle\text{FS}|$  gives rise to the mean-field decoupling. The second term generates the contributions that involve a correlation function

$$\langle\text{FS}| d_{\mathbf{k}\downarrow} d_{\mathbf{p}\downarrow}^\dagger(t) c_{\mathbf{q}}^\dagger c_{\mathbf{p}+\mathbf{q}-\mathbf{k}} |\text{FS}\rangle. \quad (44)$$

The consideration of the calculation of this correlation function is left for future work, with which one may recover the variational results presented in Ref. [27].

*Note added.* Recently, we were informed by Wasak of their interesting related theoretical work [42], in which the decoherence and momentum relaxation in Fermi-polaron Rabi dynamics are analyzed by a kinetic equation approach. Excellent agreement between their theoretical predictions and the LENS experimental data was demonstrated, without any free parameters. The connection and comparison between our work and their theoretical analysis are beyond the scope of

the present work. We note also that a strongly driven Fermi polaron was recently realized experimentally [43], which motivates us to develop a more accurate theory of Fermi spin polarons beyond the many-body  $T$ -matrix approximation and a better description of Rabi dynamics than the current mean-field decoupling approach.

#### ACKNOWLEDGMENTS

This research was supported by the Australian Research Council's Discovery Program, Grants No. DP240101590 (H.H.) and No. DP240100248 (X.-J.L.). X.-J.L. was also supported in part by the National Science Foundation under Grant No. PHY-1748958.

#### APPENDIX: THE TWO-PARTICLE VERTEX FUNCTION WITHIN THE LADDER APPROXIMATION

The diagrammatic representation of the two-particle vertex functions is shown in Fig. 12. For  $\Gamma_{11}(Q)$  in Fig. 12(a) and  $\Gamma_{21}(Q)$  in Fig. 12(c), we can write

$$\Gamma_{11}(Q) = g_1 - g_1 \tilde{\chi}_{11}(Q) \Gamma_{11} - g_1 \tilde{\chi}_{12}(Q) \Gamma_{21}, \quad (\text{A1})$$

$$\Gamma_{21}(Q) = -g_2 \tilde{\chi}_{21}(Q) \Gamma_{11} - g_2 \tilde{\chi}_{22}(Q) \Gamma_{21}, \quad (\text{A2})$$

with the pair propagators  $\tilde{\chi}_{ij}$  ( $i, j = 1, 2$ ) defined in Eq. (10). By solving these two equations, we find that

$$\Gamma_{11}(Q) = \frac{1/g_2 + \tilde{\chi}_{22}}{(1/g_1 + \tilde{\chi}_{11})(1/g_2 + \tilde{\chi}_{22}) - \tilde{\chi}_{12}\tilde{\chi}_{21}}, \quad (\text{A3})$$

$$\Gamma_{21}(Q) = \frac{-\tilde{\chi}_{21}}{(1/g_1 + \tilde{\chi}_{11})(1/g_2 + \tilde{\chi}_{22}) - \tilde{\chi}_{12}\tilde{\chi}_{21}}. \quad (\text{A4})$$

We similarly solve  $\Gamma_{12}(Q)$  and  $\Gamma_{22}(Q)$  by using the diagrams in Figs. 12(b) and 12(d). It is readily seen that the final expressions for the various two-particle vertex functions can be written in a compact form, as given by Eq. (9).

- [1] A. S. Alexandrov and J. T. Devreese, *Advances in Polaron Physics*, Springer Series in Solid-State Physics, Vol. 159 (Springer, New York, 2010).
- [2] L. D. Landau, Electron motion in crystal lattices, *Phys. Z. Sowjetunion* **3**, 664 (1933).
- [3] I. Bloch, J. Dalibard, and W. Zwerger, Many-body physics with ultracold gases, *Rev. Mod. Phys.* **80**, 885 (2008).
- [4] C. Chin, R. Grimm, P. Julienne, and E. Tiesinga, Feshbach resonances in ultracold gases, *Rev. Mod. Phys.* **82**, 1225 (2010).
- [5] H. Hu, X.-C. Yao, and X.-J. Liu, Second sound with ultracold atoms: A brief review, *AAPPS Bull.* **32**, 26 (2022).
- [6] P. Massignan, M. Zaccanti, and G. M. Bruun, Polarons, dressed molecules and itinerant ferromagnetism in ultracold Fermi gases, *Rep. Prog. Phys.* **77**, 034401 (2014).
- [7] Z. Lan and C. Lobo, A single impurity in an ideal atomic Fermi gas: Current understanding and some open problems, *J. Indian Inst. Sci.* **94**, 179 (2014).
- [8] R. Schmidt, M. Knap, D. A. Ivanov, J.-S. You, M. Cetina, and E. Demler, Universal many-body response of heavy impurities coupled to a Fermi sea: A review of recent progress, *Rep. Prog. Phys.* **81**, 024401 (2018).
- [9] S. I. Mistakidis, G. C. Katsimiga, G. M. Koutentakis, and P. Schmelcher, Repulsive Fermi polarons and their induced interactions in binary mixtures of ultracold atoms, *New J. Phys.* **21**, 043032 (2019).
- [10] K. Seetharam, Y. Shchadilova, F. Grusdt, M. B. Zvonarev, and E. Demler, Dynamical quantum Cherenkov transition of fast impurities in quantum liquids, *Phys. Rev. Lett.* **127**, 185302 (2021).
- [11] A. Schirotzek, C.-H. Wu, A. Sommer, and M. W. Zwierlein, Observation of Fermi polarons in a tunable Fermi liquid of ultracold atoms, *Phys. Rev. Lett.* **102**, 230402 (2009).
- [12] Y. Zhang, W. Ong, I. Arakelyan, and J. E. Thomas, Polaron-to-polaron transitions in the radio-frequency spectrum of a quasi-two-dimensional Fermi gas, *Phys. Rev. Lett.* **108**, 235302 (2012).
- [13] C. Kohstall, M. Zaccanti, M. Jag, A. Trenkwalder, P. Massignan, G. M. Bruun, F. Schreck, and R. Grimm, Metastability and coherence of repulsive polarons in a strongly interacting Fermi mixture, *Nature (London)* **485**, 615 (2012).
- [14] M. Koschorreck, D. Pertot, E. Vogt, B. Fröhlich, M. Feld, and M. Köhl, Attractive and repulsive Fermi polarons in two dimensions, *Nature (London)* **485**, 619 (2012).
- [15] F. Scazza, G. Valtolina, P. Massignan, A. Recati, A. Amico, A. Burchianti, C. Fort, M. Inguscio, M. Zaccanti, and G. Roati, Repulsive Fermi polarons in a resonant mixture of ultracold  ${}^6\text{Li}$  atoms, *Phys. Rev. Lett.* **118**, 083602 (2017).
- [16] Z. Yan, P. B. Patel, B. Mukherjee, R. J. Fletcher, J. Struck, and M. W. Zwierlein, Boiling a unitary Fermi liquid, *Phys. Rev. Lett.* **122**, 093401 (2019).
- [17] M. Cetina, M. Jag, R. S. Lous, I. Fritsche, J. T. M. Walraven, R. Grimm, J. Levinsen, M. M. Parish, R. Schmidt, M. Knap, and E. Demler, Ultrafast many-body interferometry of impurities coupled to a Fermi sea, *Science* **354**, 96 (2016).
- [18] N. Darkwah Oppong, L. Riegger, O. Bettermann, M. Höfer, J. Levinsen, M. M. Parish, I. Bloch, and S. Fölling, Observation of coherent multiorbital polarons in a two-dimensional Fermi gas, *Phys. Rev. Lett.* **122**, 193604 (2019).
- [19] G. Ness, C. Shkedrov, Y. Florshaim, O. K. Diessel, J. von Milczewski, R. Schmidt, and Y. Sagi, Observation of a smooth polaron-molecule transition in a degenerate Fermi gas, *Phys. Rev. X* **10**, 041019 (2020).
- [20] J. Wang, X.-J. Liu, and H. Hu, Exact quasiparticle properties of a heavy polaron in BCS Fermi superfluids, *Phys. Rev. Lett.* **128**, 175301 (2022).
- [21] J. Wang, X.-J. Liu, and H. Hu, Heavy polarons in ultracold atomic Fermi superfluids at the BEC-BCS crossover: Formalism and applications, *Phys. Rev. A* **105**, 043320 (2022).
- [22] J. Wang, Functional determinant approach investigations of heavy impurity physics, *AAPPS Bull.* **33**, 20 (2023).
- [23] R. Schmidt and M. Lemeshko, Rotation of quantum impurities in the presence of a many-body environment, *Phys. Rev. Lett.* **114**, 203001 (2015).
- [24] M. Knap, D. A. Abanin, and E. Demler, Dissipative dynamics of a driven quantum spin coupled to a bath of ultracold fermions, *Phys. Rev. Lett.* **111**, 265302 (2013).
- [25] M. M. Parish and J. Levinsen, Quantum dynamics of impurities coupled to a Fermi sea, *Phys. Rev. B* **94**, 184303 (2016).
- [26] H. S. Adlong, W. E. Liu, L. D. Turner, M. M. Parish, and J. Levinsen, Signatures of the orthogonality catastrophe in a coherently driven impurity, *Phys. Rev. A* **104**, 043309 (2021).
- [27] H. S. Adlong, W. E. Liu, F. Scazza, M. Zaccanti, N. D. Oppong, S. Fölling, M. M. Parish, and J. Levinsen, Quasiparticle lifetime of the repulsive Fermi polaron, *Phys. Rev. Lett.* **125**, 133401 (2020).
- [28] R. Combescot, A. Recati, C. Lobo, and F. Chevy, Normal state of highly polarized Fermi gases: Simple many-body approaches, *Phys. Rev. Lett.* **98**, 180402 (2007).
- [29] H. Hu, B. C. Mulkerin, J. Wang, and X.-J. Liu, Attractive Fermi polarons at nonzero temperatures with a finite impurity concentration, *Phys. Rev. A* **98**, 013626 (2018).
- [30] J. Wang, X.-J. Liu, and H. Hu, Roton-induced Bose polaron in the presence of synthetic spin-orbit coupling, *Phys. Rev. Lett.* **123**, 213401 (2019).
- [31] B. C. Mulkerin, X.-J. Liu, and H. Hu, Breakdown of the Fermi polaron description near Fermi degeneracy at unitarity, *Ann. Phys. (NY)* **407**, 29 (2019).
- [32] H. Tajima and S. Uchino, Thermal crossover, transition, and coexistence in Fermi polaronic spectroscopies, *Phys. Rev. A* **99**, 063606 (2019).
- [33] H. Tajima, J. Takahashi, S. I. Mistakidis, E. Nakano, and K. Iida, Polaron problems in ultracold atoms: Role of a Fermi sea across different spatial dimensions and quantum fluctuations of a Bose medium, *Atoms* **9**, 18 (2021).
- [34] H. Hu, J. Wang, J. Zhou, and X.-J. Liu, Crossover polarons in a strongly interacting Fermi superfluid, *Phys. Rev. A* **105**, 023317 (2022).
- [35] H. Hu and X.-J. Liu, Fermi polarons at finite temperature: Spectral function and rf spectroscopy, *Phys. Rev. A* **105**, 043303 (2022).
- [36] H. Hu, J. Wang, and X.-J. Liu, Thermally stable  $p$ -wave repulsive Fermi polaron without a two-body bound state, *AAPPS Bull.* **33**, 27 (2023).
- [37] F. Chevy, Universal phase diagram of a strongly interacting Fermi gas with unbalanced spin populations, *Phys. Rev. A* **74**, 063628 (2006).

- [38] X. Cui and H. Zhai, Stability of a fully magnetized ferromagnetic state in repulsively interacting ultracold Fermi gases, *Phys. Rev. A* **81**, 041602(R) (2010).
- [39] M. M. Parish and J. Levinsen, Highly polarized Fermi gases in two dimensions, *Phys. Rev. A* **87**, 033616 (2013).
- [40] H. Hu, J. Wang, R. Lalor, and X.-J. Liu, Two-dimensional coherent spectroscopy of trion-polaritons and exciton-polaritons in atomically thin transition metal dichalcogenides, *AAPPS Bull.* **33**, 12 (2023).
- [41] W. E. Liu, J. Levinsen, and M. M. Parish, Variational approach for impurity dynamics at finite temperature, *Phys. Rev. Lett.* **122**, 205301 (2019).
- [42] T. Wasak, M. Sighinolfi, J. Lang, F. Piazza, and A. Recati, Decoherence and momentum relaxation in Fermi-polaron Rabi dynamics: A kinetic equation approach, [arXiv:2205.05941](https://arxiv.org/abs/2205.05941).
- [43] F. J. Vivanco, A. Schuckert, S. Huang, G. L. Schumacher, G. G. T. Assumpção, Y. Ji, J. Chen, M. Knap, and N. Navon, The strongly driven Fermi polaron, [arXiv:2308.05746](https://arxiv.org/abs/2308.05746).